ATMOSPERIC MICROWAVE PLASMA TREATMEMT ON OIL-CONTAMINATED ALUMIUM SURFACE

By

Weikun Zhu

Senior Thesis in Electrical Engineering

University of Illinois at Urbana-Champaign

Advisor: Professor David N. Ruzic

May 2018

Abstract

An atmospheric microwave plasma was used to clean and activate oil-contaminated Al surfaces. Treatment was done on a large-area basis by moving the desired sample over an atmospheric pressure plasma torch. The cleaning effectiveness is supported by contact angle measurements, ATR-FTIR, SEM, XPS, and a water-break free test. In addition, the effect of processing parameters on the result of surface cleaning and activation was studied. An enhancement of surface hydrophilicity was observed as a result of increasing input microwave power and plasma exposure time. The effect of surface temperature on plasma treatment was investigated through comparing water contact angles of two methods of plasma treatment with identical exposure time, power, and gas composition. Moreover, spatially resolved ATR-FTIR spectrums from partially cleaned surfaces reveal the extent of oxidation across the plasma treated area.

Subject Keywords: Atmospheric plasma, microwave plasma, aluminum alloy surface treatment

Acknowledgments

This project was funded by the Strategic Environmental Research and Development Program (SERDP), Project Number: WP-2742.

Contents

1. Introduction

Aluminum and its alloys, due to their large strength-to-weight ratio, had been used as the construction material of modern aircrafts. The metal would be corroded under humid conditions, and therefore, a corrosion resistive layer is usually applied on top of aluminum surfaces. The U.S. Air Force generally adopted an organic coating system, including a chromate conversion coat, an epoxy resin primer, and a polyurethane topcoat [1]. In both cases the conversion coating and primer exist chemicals containing chromium ion in its +6 oxidation state, or hexavalent chromium (Cr(VI)). Hexavalent chromium is known as a respiratory carcinogen and allergen, threating the health of workers exposed to airborne Cr(VI). In addition, Cr(VI)-polluted water causes environmental issues as well as affecting kidney functions through ingestion [2]. Research efforts are employed to investigate approaches to reduce Cr(VI) [3], as well as finding alternative means to achieve corrosion protection [4]. Apart from the coating processes, the cleaning of oil-contaminated metal surfaces needs equal attention, as a lacking a proper cleaning will affect the adhesion and bonding capability of aluminum.

Atmospheric plasma processing can offer both cleaning and coating processes. Plasma from its nature can not only treat fat surfaces, but also can treat surfaces with curvatures. Recently, Bonova et. al. demonstrated the Diffuse Coplanar Surface Barrier Discharge plasma source to successfully clean the oil-contaminated aluminum surface. [5] Thin film deposition of atmospheric pressure plasma jet was also demonstrated. [6] Other atmospheric pressure plasma systems, such as radio frequency plasma torch and plasma-energized jet, had been employed to treat metallic surfaces [7,

8]. Among them, microwave plasma demonstrated advantages regarding to its economic-viable power sources.

Herein, we report an atmospheric plasma treatment of oil-contaminated aluminum alloy surfaces. The cleaning and surface activation results were assessed by contact angle measurements, ATR-FTIR, and XPS. In addition, the impact of processing parameters on the wettability of the treated surface was investigated though contact angle measurements. Moreover, spatial-resolved ATR-FTIR offers insights on the state of oxidation of oil across the plasma treated area. We further proved our large-area processability of cleaning and surface activation through treating a 1-by-1-inch surface and subsequently demonstrated the surface hydrophilicity through contact angle measurement and water break-free test.

2. Literature Review

2.1 Overview of ECAP Instrument

The evaporative coating at atmospheric pressure (ECAP) was developed in the Center for Plasma - Material Interaction (CPMI) by Wu et al. [9] based on the setup demonstrated by Ouyang et al. [10]. The essential idea is to use a microwave power source to strike a plasma at atmospheric pressure. Such atmospheric plasma, when ignited in a carefully chosen gas, such as nitrogen, will produce a high temperature plasma flame (1400 °C at 1350 W according to COMSOL simulation) that is capable to evaporate metals and deposit them in an atom-by-atom fashion on a substrate. Deposition of aluminum oxide was demonstrated with similar morphologies produced by common low-pressure processes such as DC reactive sputtering with two orders of magnitude higher deposition rate.

ECAP utilizes an atmospheric pressure plasma torch (APPT). A schematic of APPT is shown in Figure 2.1. The torch implements three coaxial hollow cylinders with decreasing diameters approaching the top of the troch. In the center of the torch, a tungsten antenna is connected to a microwave coupler, where the microwave is delivered from a microwave power supply. Between the outer cylinders and antenna exists a quartz tube to regulate the flow profile of the inlet gas, as well as prevent arcing from the antenna to the torch body. The power of the input microwave can be adjusted up to 10 kW. A tuner section is contained in the microwave waveguide so that one can tune the reflected power to zero. Plasma gas enters at the bottom of the torch and flows to the tip of the antenna, where the plasma is ignited and maintained. The target metal can be inserted inside the cup of the antenna tip, where the metal is being evaporated by the plasma and deposited on the desired substrate.

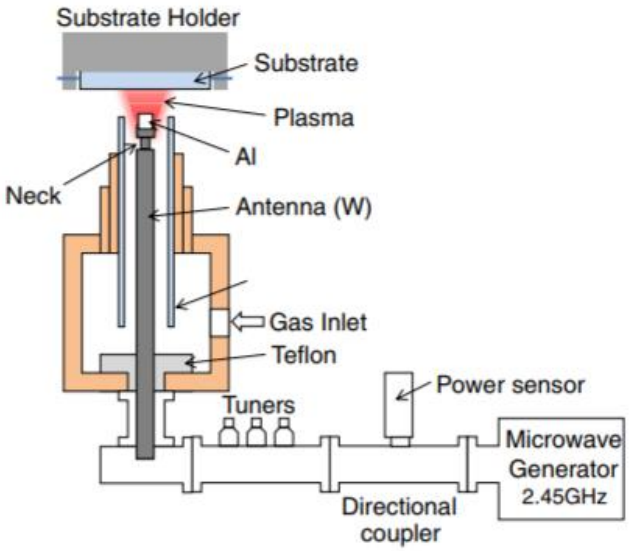

Figure 2.1. Schematic of the atmospheric pressure plasma torch [9].

2.2 Previous Works of Atmospheric Plasma Cleaning

Atmospheric plasma treatment of oil contaminated Al surface was first demonstrated by Bonova et al. [5], where a Diffuse Coplanar Surface Barrier Discharge (DCSBD) setup was utilized. The setup contains a set of coplanar electrodes with a sample holder rail on top of the electrodes. Oxygen plasma is generated between the space of the electrode and sample holder rail. Cleaning of the sample is achieved by passing a sample across the electrodes in a fixed amount of time (from 1 sec to 60 sec). Oil was introduced to the Al sample surface using spin coating and was exposed to oxygen plasma. The contact angle of the Al surface was immediately reduced to 10° after treating the surface for 1 sec, suggesting enhanced surface hydrophilicity. An ATR-FTIR spectrum was recorded before and after cleaning; the evidential carbon-hydrogen vibrational peak before cleaning disappeared after plasma treatment, indicating successful removal of the oil layer. XPS was employed to characterize the chemical state of C 1s, N 1s, and Al 2p. The results confirm the

removal of contaminated oil and indicate an enhancement of surface hydroxy groups and surface nitrite formation.

While DCSBD provides fast and efficient treating of Aluminum surfaces, its setup restricts its cleaning potential to curved surfaces. Munoz et al. developed a surface-wave discharge atmospheric plasma and studied the cleaning potentials of the post-discharge region of the plasma [11]. The plasma was powered by a 2.45 GHz microwave power source, and samples are passed through the post-discharge region of the plasma, a region that extends beyond the glowing plasma blob while still retaining radical populations, offering both radicals for cleaning and low temperature to prevent surface damage of metals. The water contact angle of an argon plasma cleaned surface is 21°. By introducing 2% of nitrogen content into the argon flow, the water contact angle was further reduced to 7°. The post-discharge region can activate the surface until 6 cm from the nozzle. Collected XPS data confirms the implantation of surface hydroxyl group as the mechanism of increased surface hydrophilicity.

2.3 Surface Characterization Methods

2.3.1 Contact Angle Measurement

Contact angle is a commonly employed technique to determine the wettability of a solid surface. Contact angle θ_c can be obtained by dropping a liquid on to a solid surface, and measuring the angle formed by the tangential line of the liquid curve front and the solid plane. A schematic of a liquid droplet on a solid surface is shown in Figure 2.2. Through a force balance on the horizontal direction, the Young Equation can be derived (Equation 1), where γ_{SL}, γ_{LG}, and γ_{SG} corresponds

to the interfacial energy of the solid-liquid interface, liquid-gas interface, and solid-gas interface, respectively. The contact angle is related to the work of adhesion W_{SL} of the solid through Young-Dupre equation (Equation 2), where γ_L is the interfacial energy of the liquid. A small contact angle θ_c infers to a higher work of adhesion and a more hydrophilic surface. A large contact angle denotes a lower work of adhesion and therefore a more hydrophobic surface.

$$\gamma_{SG} - \gamma_{SL} - \gamma_{LG}\cos(\theta_c) = 0 \quad (1)$$

$$W_{SL} = \gamma_L(1+\cos(\theta_c)) \quad (2)$$

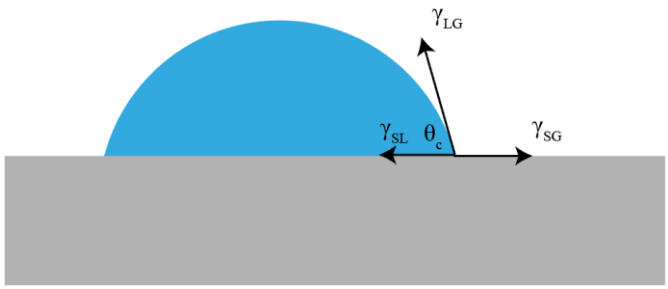

Figure 2.2. A schematic of a liquid drop on a solid surface. θ_c refers to the contact angle of the liquid droplet, and γ_{SL}, γ_{LG}, and γ_{SG} corresponds to the interfacial energy of the solid-liquid interface, liquid-gas interface, and solid-gas interface, respectively.

2.3.2 Water-Break Free Test

The water-break free test (ASTM F22-13) [12] is a standard test method for hydrophobic surface films. The test is conducted by withdrawing the test surface vertically from water. A contained area of the film having a surface tension lower than water will result water to bead up at the contaminated locations. Such bead up will be manifested through "break" while draining the water,

indicating hydrophobic contaminants. If no breakage is observed, there are no surface hydrophobic contaminants.

2.3.3 Attenuated Total Reflection Fourier Transform Infrared Spectroscopy (ATR-FTIR)

Infrared spectroscopy measures the vibrational modes of a molecule. It is commonly used for detecting functional groups of organic compounds. For a vibrational mode to be active, it must involve a change in dipole moment. There are radial, latitudinal, and longitudinal stretching, both symmetric and asymmetric. The wavelengths to excite these vibrational modes reside in the range of infrareds. Individual functional groups exhibit disparate excitation wavelengths, and therefore an IR spectrum would inform a reader about disparate groups within a molecule. For instance, a hydroxyl group usually results in an absorption peak from 3400 cm^{-1} to 3700 cm^{-1}.

To obtain an IR spectrum, a Fourier Transform Infrared (FTIR) spectroscopy technique is usually employed. FTIR utilizes a Michelson interferometer, where a motorized moving mirror modulates constructive or destructive interference of each wavelength. A plot of received light intensity as a function of mirror offset distance will be obtained. After converting the mirror offset difference into moving time and applying a fast Fourier transform, one will attain a FTIR spectrum.

FTIR is commonly used to measure IR absorption or transmission spectrum of gas, solid, and liquid. If the state of chemical bonds on a surface or film is of interest, attenuated total-reflection Fourier transform infrared (ATR-FTIR) spectroscopy is used. The technique utilized the

evanescent field of a total internal-reflected electromagnetic wave. The setup uses a crystal having a high refractive index. The crystal is brought close to the sample surface, where a beam of infrared wave having an incident angle greater than the critical angle is shined from the crystal side. This condition satisfied total internal reflection, therefore an evanescent wave (an exponential decay wave) is generated and extends to the sample medium. The penetration depth of the evanescent wave depends upon the refractive index of the sample, typically ranging between 0.5 and 2 μm. This allows the FTIR spectrum to merely respond to the surface properties rather than those of the bulk.

2.3.4 X-ray Photoelectron Spectroscopy

X-ray photoelectron spectroscopy (XPS) is a surface characterization technique that measures the chemical state and elemental composition of a material. During an XPS measurement, a beam of X-ray is irradiated to the sample, and a detector collects the escaped electrons from the top 0 to 10 nm of the surface of the material. To ensure the escaped electron reaches the detector, an ultra-high vacuum ($P \sim 10^{-9}$ mbar) condition is required for the XPS chamber. The kinetic energies of the escape electrons are recorded with their populations. The kinetic energy recorded by the detector is converted to the binding energy, the minimum energy required to remove an electron from an atom. Each atom has its own characteristic binding energy, and therefore has distinct spectral peaks. In the same atom, different electron configurations (1s, 2s, 2p, etc.) will also result to difference in binding energies. Therefore, the surface chemical state of elements is revealed by examining the peak position of XPS spectrum. As only up to 10 nm of the material is detected, XPS spectrum will be a strong indicator of the cleanliness of a plasma treated surface in our work.

3. Results and Discussion

To investigate the effect of cleaning, an oil layer was coated on every sample prior to plasma exposure. An example of a plasma treated sample is shown in Figure 3.1a. It shows that a clear track of oil is being removed from the sample. The boundary of the track appeared to be not as linear as the movement trajectory. This is consistent with the process of cleaning, as the plasma flame resides for a longer time at the edges of the sample comparing to the middle regions. This resulted the width of the track close to the edge of the sample is wider than that in the middle of the sample.

To confirm that the microscopic morphology did not change during the duration of plasma exposure, an oil-coated sample was passed to a 600 W plasma flame whose inlet gas is composed of 20 L/min of air in 10 sec. The morphology of a representative as-received (prior to oil coating) mirror-polished sample is shown in Figure 3.1b, while that of the plasma treated surface is shown in Figure 3.1c. From the SEM images, the morphology is not influenced by the plasma exposure. The energy-dispersive X-ray spectroscopy results from the location of Figure 3.1b and 3.1c show a decrease of carbon elemental concentration from 8.2 wt% (as-received) to 6.7 wt% (plasma-treated), implying that plasma is removing the surface carbon element in addition of the removal of introduced oil coating.

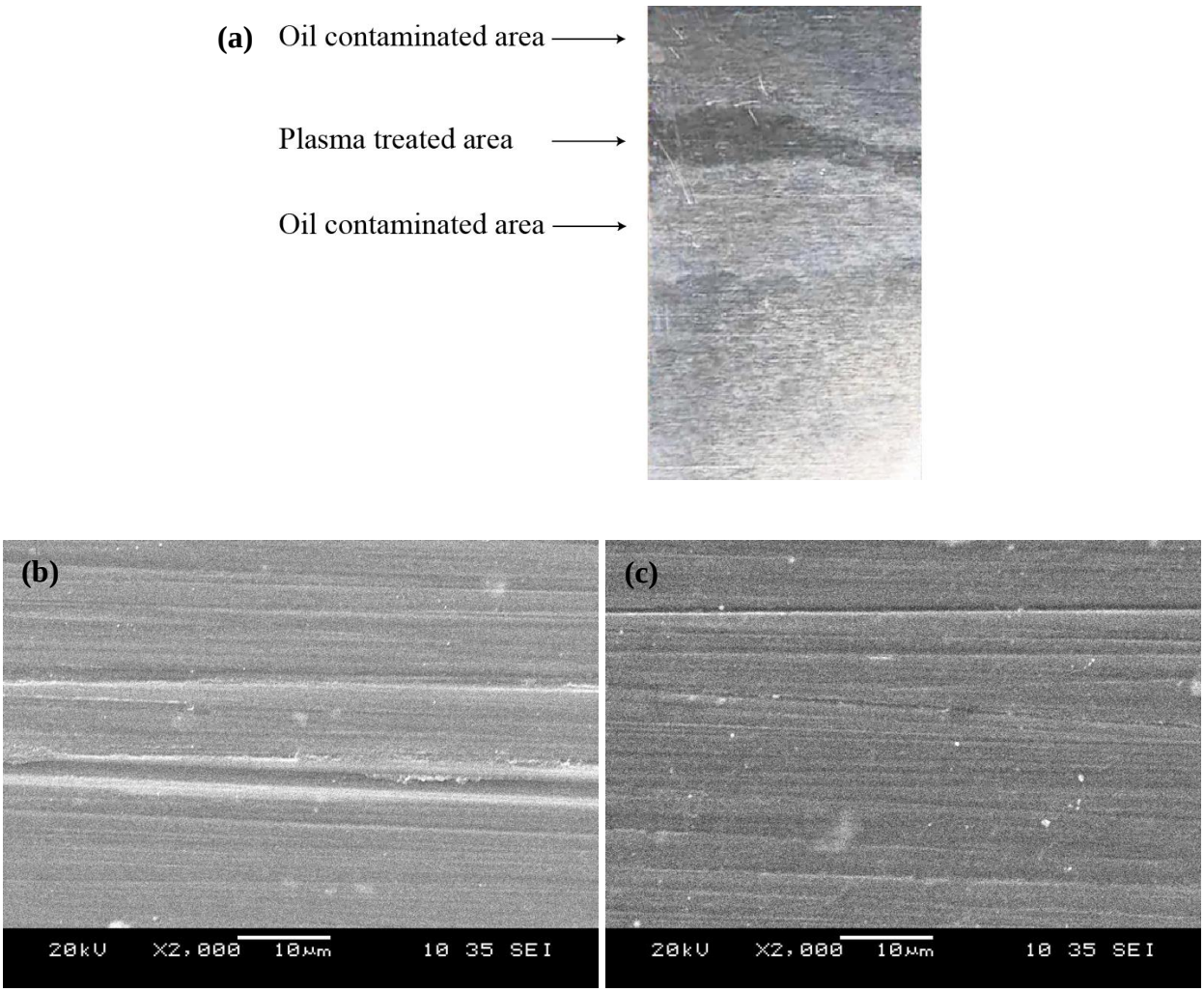

Figure 3.1. Photograph of (a) plasma treated sample, (b) SEM image of as received Al surface, and (c) SEM image of plasma cleaned surface.

To quantify the amount of oil removed from the surface, XPS, ATR-FTIR, and contact angle measurements were performed. The surface elemental composition is examined by XPS. XPS data of pump oil coated Al surface, isopropyl alcohol (IPA) cleaned surface and plasma cleaned surface after chemical cleaning are visualized in Figure 3.2. The peak at 285 eV denotes the existence of C-C single bond, whereas the peaks at 286.2 eV and 288.7 eV refer to C-O single bond and ester group, respectively. After IPA or IPA and plasma cleaning, the C-C peak for both cases decreased.

Moreover, the C-O peaks were substituted by smaller ester group peaks with similar peak intensities. It is unknown why chemically cleaning gives additional ester group peaks; one possible source might come from IPA that is responsible for cleaning, which may contain a trace of other chemicals responsible for the esters.

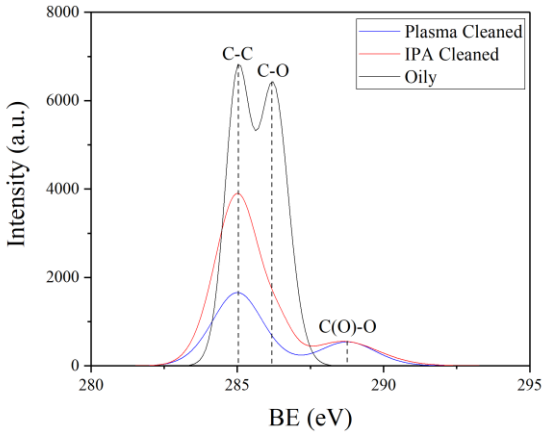

Figure 3.2. C 1s XPS spectrum of IPA cleaned, IPA and plasma cleaned, IPA and plasma cleaned (600 W microwave input power, 20 L/min of Ar and 10 L/ min of compressed air, a moving speed of 0.03 inch/s) oil-contaminated surfaces. Due to consideration of maintaining ultra-high vacuum environment, a vacuum-compatible oil was used for all XPS experiments that differs from the rest of experiments.

Peak fitting was performed for each spectrum in Figure 3.2 at binding energies of 285 eV (C-C), 286.2 eV (C-O), and 288.7 eV (C(O)-O). The fitting results are shown in Table 1. The peak area of C-C (258 eV) decreased dramatically after plasma treatment, but not necessarily after chemical treatment. This demonstrates the power of plasma to remove surface organics. In addition, through comparing the composition of C-O (286.2 eV), and C(O)-O (288.7 eV) for chemical treated and plasma treated sample, it is seen that their composition sums are similar. This infers that plasma oxidized the C-O group into C(O)-O.

Table 1. C 1s peak fitting results of oil-contaminated surface, plasma treated surface, and chemical treated surface.

	Peak Area at 285 eV	Composition at 285 eV	Peak Area at 286.2 eV	Composition at 286.2 eV	Peak Area at 288.7 eV	Composition at 288.769 eV
Oil-contaminated	6972	46.2%	8125	53.8%	0	0
Chemical treated	7443	74.9 %	880	8.9%	1612	16.2%
Plasma treated	3614	72.8%	0	0	1353	27.2%

Contact angle measurement was employed to assess the surface hydrophilicity of the plasma surface. Water droplets are deposited on surface with various conditions, and contact angles were measured. An image of the droplet on an as-received surface is shown in Figure 3.3a, and that of a plasma treated surface is demonstrated in Figure 3.3b. Together, they demonstrate an increase of surface hydrophilicity.

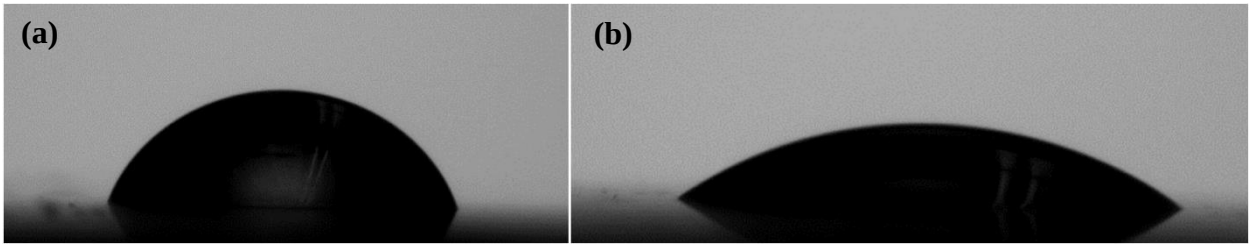

Figure 3.3. Contact angle image of (a) as-received surface and (b) plasma cleaned surface. The plasma processing condition is 600 W of microwave power, an air flow of 20 L/min, and a speed of 0.1 inch/sec.

To optimize the conditions for high surface hydrophilicity as well as a small processing time, the parameter space was examined by changing three parameters in a controlled experiment setting: power, passing time, and number of passes. The effect of each parameter is illustrated in Figure 3.4a through 3.4c. Figure 3.4d shows the aging effect of the surface over a period of 24 hours.

The effect of the microwave power input is shown in Figure 3.4a. As power gradually increases from 400 W to 800 W, the contact angle of the cleaned surface drops from 60º to 20º, indicating a rise in hydrophilicity. An increase of power leads to an enhancement of the temeprature of the plasma, thereby the surface reaction rate and a higher density of hydroxy group formation in a fixed amount of time, which gives rise to a drop in contact angle. It is worth noting that the plasma at 400 W exhibits a small capacity of cleaning, as the measured contact angle is near that of the oil-contaminated surface. This is confimed visually by observing that cleaned surface remains oily. From 500 W on, the higher power plasma flame gives a fully cleaned track. As power increases to 700 W, the contact angle saturated.

Next, the effect of exposure time is examined through two parameters side by side: single track passing time and number of passes. The single track passing time is defined by the time the plasma flame is in contact with the sample. For the samples used in this project, by assuming the plasma source as a point source, the passing time can be determined through divding the width of the sample (1 inch) by the moving speed of the sample set by the user. Alternatively, the exposure time can be varied by setting a small single track passing time, and pass the sample mutiple times at the same location. For the same amount of plasma exposure time, the mutiple passes method gives a smaller temperature rise since the sample passes faster each time and has additional time

to cool down. This is proven by measuring maximum temperature of the sample experience as it was treated by the plasma: the maxiumum temperature for a single 20 sec exposure is 383.8 ºC and that of the double 10-sec-pass is 193.1 ºC. Figure 3.4b shows the contact angle evolution as a function of passing time, whereas Figure 3.4c shows the effect of number of passes; each pass in Figure 3.4c lasts for 10 sec. Both plots demonstrated a decrease of contact angle as passing time/number of passes increases. Comparing a single track passing time of 20 sec to two passes, and a single track passing time of 60 sec to six passes, it can be seen that the contact angles of both two passes and six passes outperform those single passes having an identical plasma exposure time.

Last but not least, the aging effect of conatct angle is examined by treating samples at the same condition and measuring their contact angles at different period of times. The evolution of contact angle was examined from 1 hr to 24 hr after the plasma treatment. The resulting change in contact angle is shown in Figure 4d. The contact angle increased from 26º to 33º as the aging time evolves from 1hr to 24 hr. The small increase in contact angle over a day indicates stability of the surface after plasma treatment.

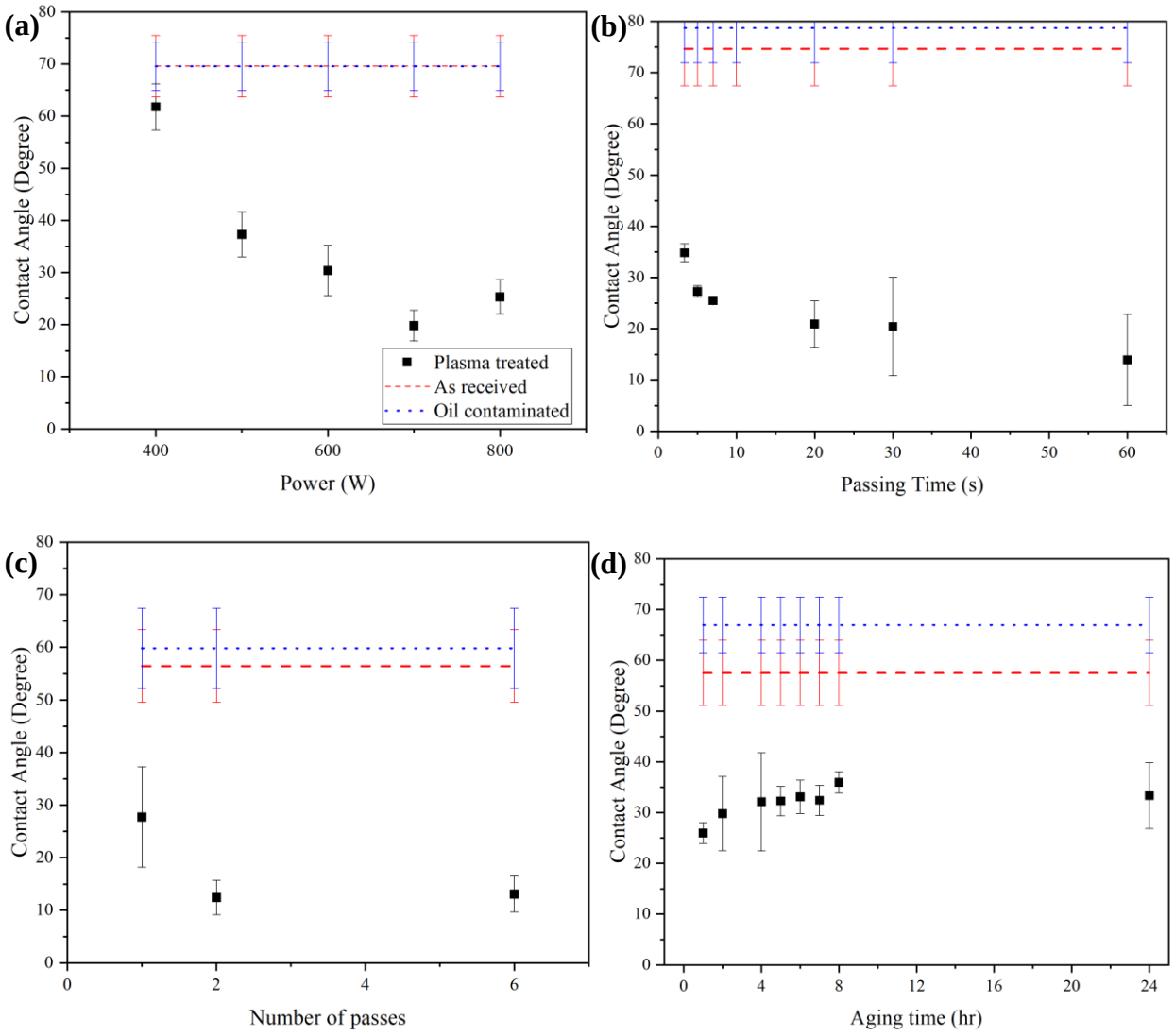

Figure 3.4. Contact angle evolution as a function of (a) microwave power supply's power, (b) treating time of the sample per track, (c) number of repeating treatment (10 sec per single pass) of the same area, and (d) post-plasma-treating time.

To study the evolution of chemical composition of the cleaning process, ATR-FTIR was employed to examine Al sample surface prior and after cleaning. Figure 3.5 showed the FTIR spectrum of an oil-contaminated surface, and two plasma treated surface spectrum with different passing time. Initially, for the oil-contaminated surface without plasma exposure, only C-H vibrational peaks are present, indicating that there are only carbon hydrates in the initial system. After 3.3 sec of

plasma exposure with a power of 600 W and a gas composition of 20 L/min of air, the intensity of C-H peaks decreases significantly, signifying that an amount of oil is removed. In addition, carbon-carbon double bond and carbonyl peak emerged as an intermediate product of the oxidation process. After the sample had been exposed by plasma for 10 sec with otherwise identical conditions, all of the peaks had disappeared, which denotes a complete removal of oil layer. Yet, a removal of oil layer does not indicate a large surface hydrophilicity, as the condition for oil removal correspond to a surface contact angle of 30º, whereas the sample that passes the water break free test had a contact angle of 5º (See Water-Break Free Test). Therefore, to achieve optimal surface hydrophilicity, one needs to treat the surface further after oxidizing the oil on the surface.

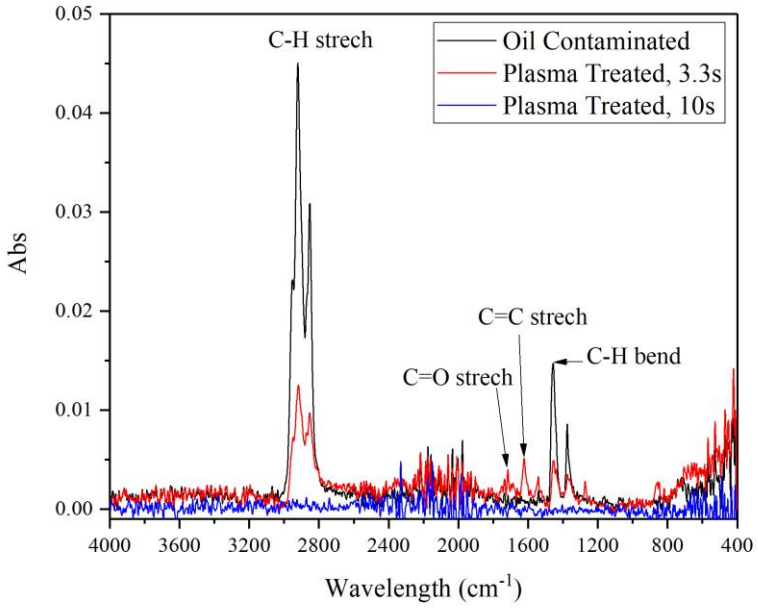

Figure 3.5. ATR-FTIR spectrum of plasma cleaned surface.

Figure 3.5 offers information on the emergence of new IR vibrational peaks and ultimately the disappearance of all vibrational peaks as the plasma is treating the oil-contaminated surface. However, it misses the spatial distribution of chemical bonding states of the oil after plasma cleaning. As the cleaning track of the plasma is finite, one would expect more oils are oxidized at the center of the track compared to those at the peripheral. We confirmed this hypothesis through spatially resolved ATR-FTIR to scan across the cleaned track. The instrument window size of 0.1 inch by 0.1 inch gives an incremental sampling distance of 0.1 inch. A schematic is shown in Figure 3.6a. Two samples were exposed in the plasma at a power of 400 W and a gas composition of 20 L /min but in different plasma exposure times to obtain partially treated tracks so that the extent of oxidation can be examined. Integration was performed for two peaks representing vibration peaks of C=C streching (centered at 1625 cm^{-1}, integrated from 1575 cm^{-1} to 1665 cm^{-1}) and C-H bending (centered at 1454 cm^{-1}, integrated from 1400 cm^{-1} to 1490 cm^{-1}). Subsequently, the peak integral ratio was calculated by dividing the C-H integral by the C=C peak integral, and was plotted as a function of position across the cleaned tracks of four different plasma exposure times in Figure 3.6b.

Several trends can be inferred from Figure 3.6b. First, for both exposed sample, a maximum ratio is observed at the center of the envelop, indicating that more oils are being oxidized at the center of the clean track than at the periphery. Second, the peak ratio maximum of 20 sec plasma exposure is greater than 5 sec plasma exposure, inferring a higher degree of oxidation as the exposure time increases. Third, the width of the envelop widens as exposure time increases, indicating the plasma flame is affecting a border region as exposure time elevates.

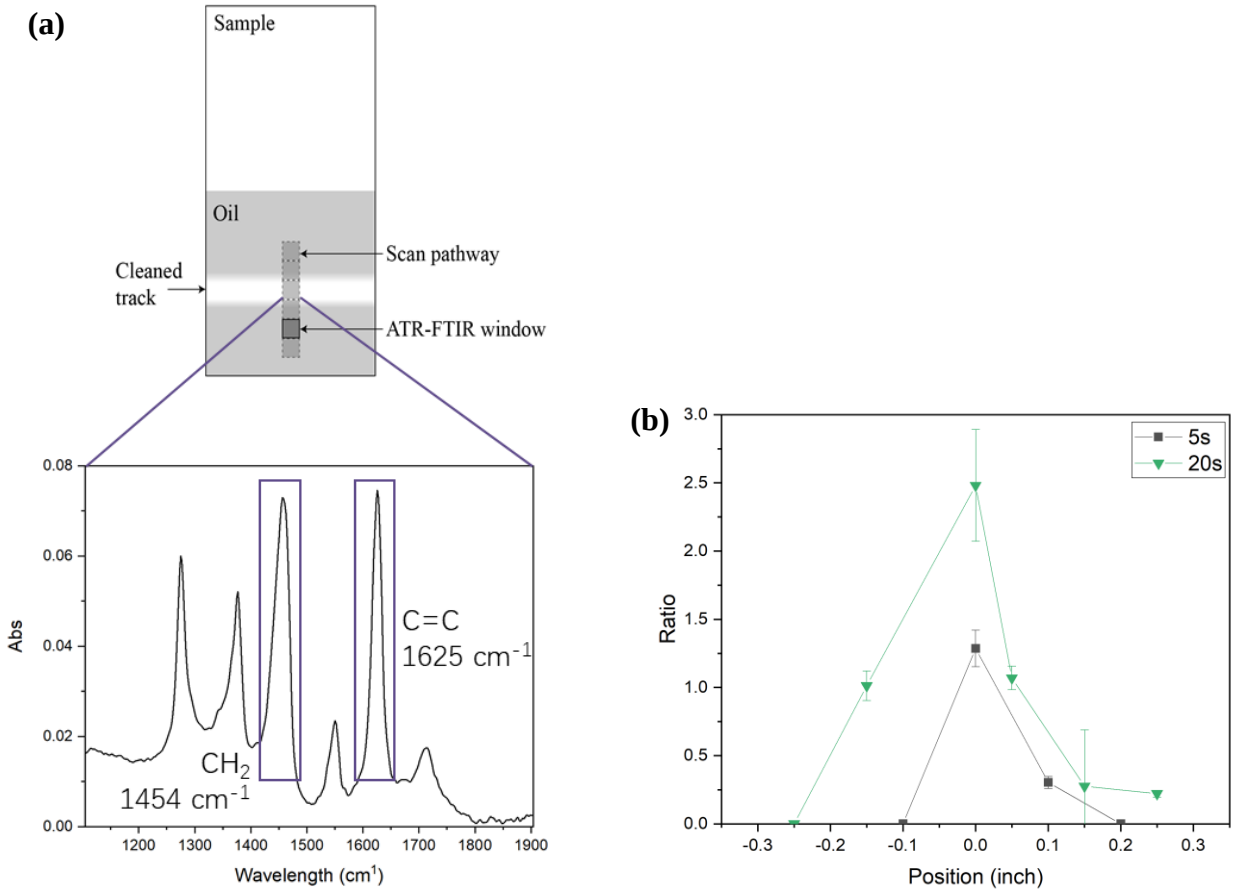

Figure 3.6. (a) Schematic of ATR-FTIR's measurement on the spatial distribution of oil bonding state and a zoomed sample spectrum from 1100 cm^{-1} to 1900 cm^{-1} with the C-H bending peak and C=C stretching peaks labeled. (b) Peak integral ratio of C=C peak (1625 cm^{-1}) over C-H peak (1454 cm^{-1}) as a function of position across the cleaned track and plasma exposure time. The maxima of each envelop was aligned at the position of 0 inch.

Water-Break Free Test

The goal of the project is to apply the atmospheric plasma processing technique to a larger area. To test the surface hydrophilicity for a large area sample, the water break free test was utilized by submerging the cleaned sample in DI water, pull it out and wait for 1 min for water on the surface to settle down. The water break free test is passed when no water droplets are formed in the cleaned area. To demonstrate the large-area cleaning capability, a 1-by-1-inch square portion was cleaned

in eight passes with a tilting angle of 11º. An image of the cleaned sample after pulling from DI water on the surface is shown in Figure 3.6. It can be seen that no water droplets had been formed, suggesting successful enhancement of hydrophilicity. A water contact angle of less than 5º was observed for another sample treated at identical conditions.

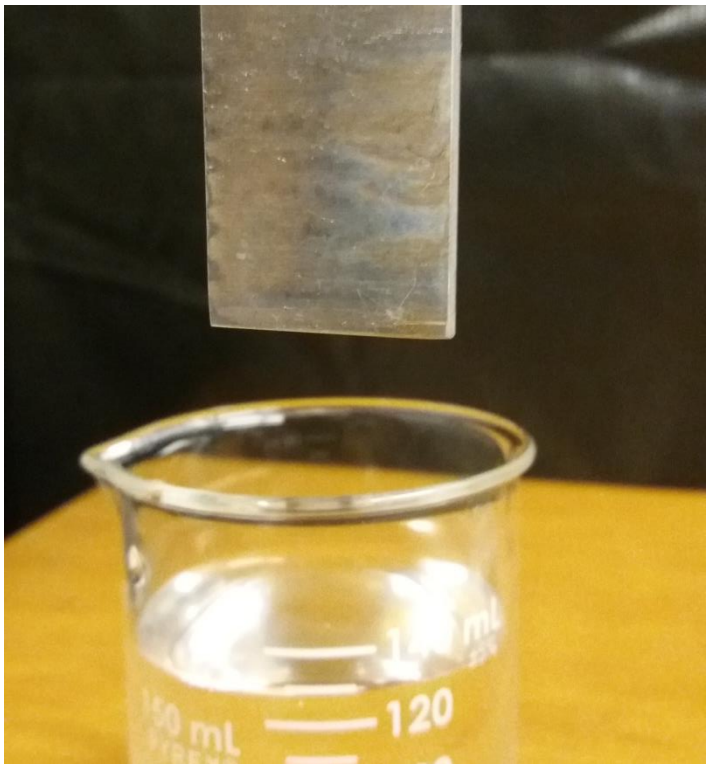

Figure 3.6. Illustration of water break free test.

4. Experimental

Experimental Setup

The setup of the torch is identical with previous work [9]. To obtain a large cleaning area, two motorized stages (Thor Lab, NRT150) enable the sample to move in the xy-plane. The movement of the stage can be controlled through the Kinetics program (version 1.14.6.0) developed by Thor Lab. A sample holder extends from the base of the motorized stage to the location of the torch, where the sample is located. A schematic is shown in Figure 4.1a. The x-direction stage is titled upward for 11º to direct the gas flow from the torch to blow the oil during cleaning, thereby accelerating the cleaning process (see Figure 4.1b). The ECAP setup is powered by a 2.45 GHz microwave source, and the tungsten antenna was 0.2 inch in diameter and 6.45 inch in height.

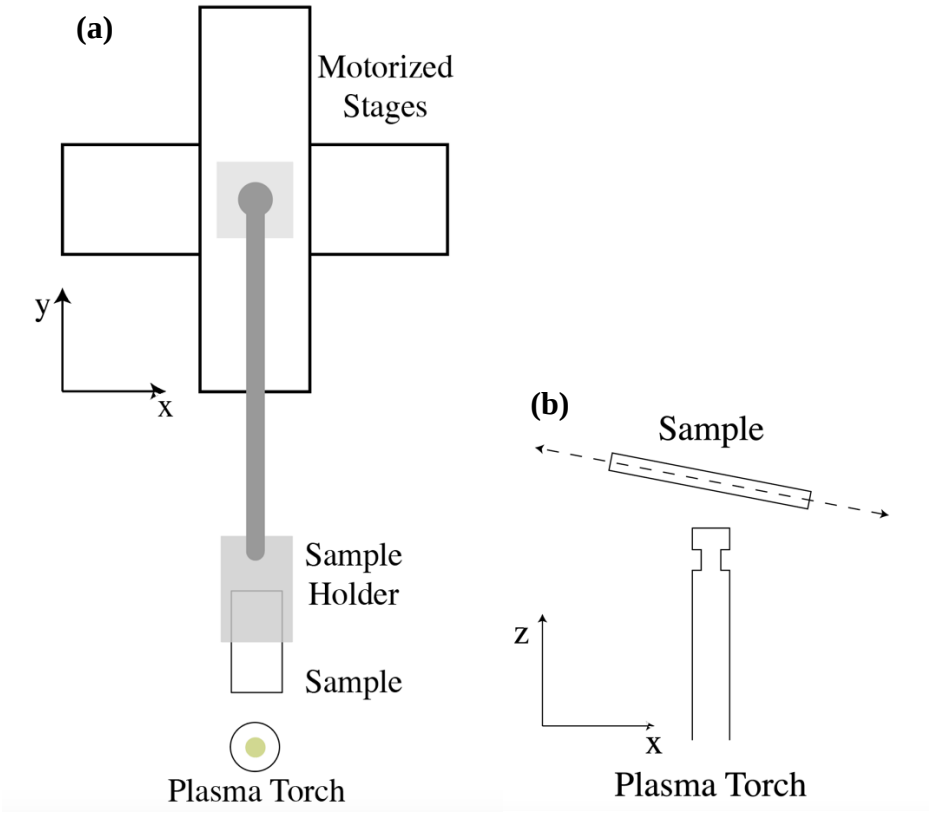

Figure 4.1. (a) Schematic of motor and sample holder setup with respect to the plasma torch. The stages can move in x and y direction. **(b)** Titled sample with respect to the torch pointing in the z

direction; the dash line refers to the moving direction of the sample. Only the antenna of the torch is visualized.

Sample Preparation

An Al 7076-T6 plate was purchased from McMaster and was cut into rectangular pieces having a length of 2 inch, a width of 1 inch, and a thickness of 0.1 inch. For the samples that undergo contact angle measurement, and FTIR, 15 µL of wt20 machine oil was casted to a 1-by-1-inch surface of the sample. The surface was rubbed with nonwoven wipers to produce a uniform layer of oil. The uniformity of the oil layer is confirmed by measuring ATR-FTIR spectrum on multiple spots of the oil-contaminated sample. For samples that were prepared for XPS, they were cleaned by toluene, acetone, and isopropyl alcohol in a supersonic chamber. Each solvent cleaning took ~ 5 min and compress air was employed to remove solvent from the sample before the next chemical was used. Chemically cleaned samples were then coated with pump oil so that the oil will not evaporate under ultra-high vacuum.

Plasma ignition and processing

The gases entering the torch, helium, argon, dry air and water saturated air, are controlled by four RMA-Mater flow meters by Dwyer. A process flow diagram of the inlet gas stream is shown in Figure 4.2.

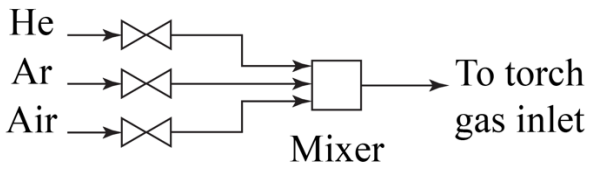

Figure 4.2. Process flow diagram of inlet gas stream.

Pure helium gas was used for plasma self-ignition with a flow rate larger than 5 L/min at a microwave power of 600 W. After plasma ignition, the processing gas was switched to air by first adding an argon stream of less than 10 L/min followed by another addition of 20 L/min of air. The Ar and He feeds were closed after the processing gas is dominated by air. From this point, the input microwave power, gas composition, and gas flow rate can be tuned accordingly.

Plasma treatment of the oil-contaminated samples are processed through passing the sample above the torch at a given speed. The sample starts from a higher location and proceed with a tilting angle of 11º to a lower location (see Figure 4.1b). The distance between the lowest point of the sample above the torch and the top surface of the second coaxial cylinder is held constant at 0.45 inch. Generally, the sample only passed once through the plasma. For large-area cleaning demonstration and to perform the water break free test, the sample passed the plasma several times to increase the cleaned area. A schematic of the trajectory of the sample is shown in Figure 4.3.

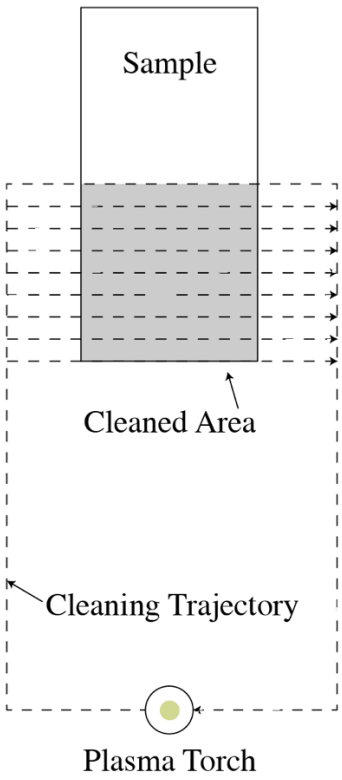

Figure 4.3. Movement trajectory of the sample, represented by the dash line. The trajectory is controlled by a sequence file output through a home-developed program in MATLAB. The gray area represents the plasma treated area.

Temperature Measurement

The temperature of the sample was determined through measuring the resistance of thermal-sensitive resistor. Thermal resistors by DigiKey (NB-PTCO-006) were glued onto the back of the sample with thermal paste between the resistor and the surface. The resistance is measured as a function of time by Dawson DDM230B Multimeter, where the resistance is recorded by a PC through the software MutiMeter developed by Dawson. A self-developed MATLAB code (see Appendix A) was used to extract the data and converting the resistance to temperature through Equation 3.

$$W_{SL} = \gamma_L (1 + \cos(\theta_c)) \quad (3)$$

Surface Characterization

The hydrophilicity of the cleaned surface was measured through contact angle measurements using Rame-Hart 250-F1 instrument. Distilled water with the volume of 1 μL was dropped onto the plasma treated and as-received surfaces, and the water contact angle was measured.

Surface composition of Al samples was analyzed by an X-ray Photoelectron Spectroscopy (XPS) system (Physical Electronics PHI 5400). Since the WT-20 oil would degas under ultra-high vacuum conditions, pump oil (Pfeiffer Balzers, P 275140203) was used as an alternative choice, and XPS was taken before after cleaning of aluminum surface. The shift of the spectrums was corrected through setting the C 1s peak at 285 eV.

The chemical bonding states on the aluminum surface was determined by attenuated total reflection Fourier Transform Infrared (ATR-FTIR) spectroscopy (Bruker ALPHA). A spectrum of air was recorded as the background. Absorption of the surface was measured, and each spectrum is the result of 24 averaged scans from 400 cm^{-1} to 4000 cm^{-1} with a resolution of 2 cm^{-1}.

The water break free test was conducted to further confirm the result of cleaning. A 1-by-1 $inch^2$ of plasma cleaned surface was obtained, and the sample was submerged into and quickly removed from DI water. The surface was held vertically, and the shape of flow was monitored closely for 1

min. The process conditions were: 600 W, 20 L/min compressed air, height of 0.45 inch, and a speed of 0.00333 inch/s. The trajectory of the sample is shown in Figure 4.3.

5. Conclusion and Future Work

In summary, we demonstrated the cleaning and activation of oil-contaminated aluminum alloy surface using an atmospheric microwave plasma process. SEM on the treated and non-treated area showed that morphology is not altered by the plasma. XPS analysis demonstrates the removal of oil layers from the surface after plasma treatment. Spatial-resolved ATR-FTIR quantifies the spatial distribution of oxidation state of the oil for various plasma exposure time. Most of the oxidation occurs in the center of the treatment area and the width of the cleaning track enhances as the exposure time increases. Contact angle measurements were utilized to investigate the effect of microwave power input, passing time, number of passes, and post-treatment time on the wettability of the treated surface. A more hydrophilic surface can be achieved by increasing power, passing time, or number of passes. Lastly, the large-area processability of the plasma was demonstrated through treating a 1-by-1 $inch^2$ of oil-contaminated Al alloy surface and performed the water break-free test to confirm its hydrophilicity.

We look forward to future research on processing parameters that we have not examined in this project, including the effect of gas flow rate and gas composition. Moreover, we hope future researchers can utilize a more spatially resolved (with window size less than 0.1 inch) instrument to examine the spatial distribution of chemical bonding state across the plasma treated region with various processing parameters conditions. Last but not the least, we look forward to conducting future work on investigating the effect of atmospheric plasma treatment on the morphology of metal surfaces through AFM and equivalent methods to expand our understanding of interaction between atmospheric plasma and surfaces.

References

[1] G. N. Carlton, "Hexavalent Chromium Exposures During Full-Aircraft Corrosion Control," *AIHA Journal*, vol. 64, pp. 668-672, 2003/09/01 2003.

[2] D. Mohan, K. P. Singh, and V. K. Singh, "Trivalent chromium removal from wastewater using low cost activated carbon derived from agricultural waste material and activated carbon fabric cloth," *Journal of Hazardous Materials*, vol. 135, pp. 280-295, 2006/07/31/ 2006.

[3] M. I. Qureshi, F. Patel, N. Al-Baghli, B. Abussaud, B. S. Tawabini, and T. Laoui, "A Comparative Study of Raw and Metal Oxide Impregnated Carbon Nanotubes for the Adsorption of Hexavalent Chromium from Aqueous Solution," *Bioinorganic Chemistry and Applications*, vol. 2017, p. 1624243, 04/10 2017.

[4] R. L. Twite and G. P. Bierwagen, "Review of alternatives to chromate for corrosion protection of aluminum aerospace alloys," *Progress in Organic Coatings*, vol. 33, pp. 91-100, 1998/02/23/ 1998.

[5] L. Bónová, A. Zahoranová, D. Kováčik, M. Zahoran, M. Mičušík, and M. Černák, "Atmospheric pressure plasma treatment of flat aluminum surface," *Applied Surface Science*, vol. 331, pp. 79-86, 2015/03/15/ 2015.

[6] Y.-w. Hsu, H.-C. Li, Y.-J. Yang, and C.-c. Hsu, "Deposition of zinc oxide thin films by an atmospheric pressure plasma jet," *Thin Solid Films*, vol. 519, pp. 3095-3099, 2011/03/01/ 2011.

[7] M. I. Boulos, "RF induction plasma spraying: State-of-the-art review," *Journal of Thermal Spray Technology*, vol. 1, pp. 33-40, 03 / 01 / 1992.

[8] Z. Cao, J. L. Walsh, and M. G. Kong, "Atmospheric plasma jet array in parallel electric and gas flow fields for three-dimensional surface treatment," *Applied Physics Letters*, vol. 94, p. 021501, 2009.

[9] Y. L. Wu, J. Hong, D. Peterson, J. Zhou, T. S. Cho, and D. N. Ruzic, "Deposition of aluminum oxide by evaporative coating at atmospheric pressure (ECAP)," *Surface and Coatings Technology*, vol. 237, pp. 369-378, 2013/12/25/ 2013.

[10] Z. Ouyang, V. Surla, T. S. Cho, and D. N. Ruzic, "Characterization of an Atmospheric-Pressure Helium Plasma Generated by 2.45-GHz Microwave Power," *IEEE Transactions on Plasma Science*, vol. 40, pp. 3476-3481, 2012.

[11] J. Muñoz, J. A. Bravo, and M. D. Calzada, "Aluminum metal surface cleaning and activation by atmospheric-pressure remote plasma," *Applied Surface Science*, vol. 407, pp. 72-81, 2017/06/15/ 2017.

[12] "Standard Test Method for Hydrophobic Surface Films by the Water-Break Test," ed.

Appendix A. MATLAB Program Converting Resistance to Temperature

```
clc

clear

close all



R_0 = 1000;

a = 3.9083e-3;

b = -5.775e-07;

c = -4.183e-12;



filename_front = '1_R_front_01302018.txt';

filename_back = '1_R_back_01302018.txt';

start_time_text = '1/30/2018\6:06:08 PM';



[index_back, variable_back, R_back, unit_back, time_back, time_AMPM_back] =
textread(filename_back,'%d %s %f %s %s %s');

[index_front, variable_front, R_front, unit_front, time_front, time_AMPM_front] =
textread(filename_front,'%d %s %f %s %s %s');



time_back = datevec(time_back,'mm/dd/yyyy\HH:MM:SS');

time_front = datevec(time_front,'mm/dd/yyyy\HH:MM:SS');



start_time = datevec(start_time_text,'mm/dd/yyyy\HH:MM:SS');

end_time_front = time_front(end,:);
```

```
end_time_back = time_back(end,:);



[~,index_start_time_back] = ismember(start_time, time_back,'rows');

[~,index_start_time_front] = ismember(start_time, time_front,'rows');



R_back_start_time_aligned = R_back(index_start_time_back : end);

R_front_start_time_aligned = R_front(index_start_time_front : end);

N_min = min(length(R_front_start_time_aligned), length(R_front_start_time_aligned));



duration_front = end_time_front(4)*3600 + end_time_front(5)*60 +end_time_front(6) -
start_time(4)*3600 - start_time(5)*60 - start_time(6);

ratio_front = duration_front/(index_front(end) - index_start_time_front);

time_front_corrected = (0: length(R_front_start_time_aligned)-1).*ratio_front;

time_front_corrected = time_front_corrected';

duration_back = end_time_back(4)*3600 + end_time_back(5)*60 + end_time_back(6) -
start_time(4)*3600 - start_time(5)*60 - start_time(6);

ratio_back = duration_back/(index_back(end) - index_start_time_back);

time_back_corrected = (0: length(R_back_start_time_aligned)-1).*ratio_back;

time_back_corrected = time_back_corrected';



ones_front = ones(length(R_front_start_time_aligned),1);

ones_back = ones(length(R_back_start_time_aligned),1);

T_front = (-R_0*a.*ones_front+sqrt((R_0*a)^2.*ones_front-4*R_0*b.*(R_0.*ones_front-
1000.*R_front_start_time_aligned))./(2*R_0*b);
```

```
T_back = (-R_0*a.*ones_back+sqrt((R_0*a)^2.*ones_back-4*R_0*b.*(R_0.*ones_back-
1000.*R_back_start_time_aligned))).*/(2*R_0*b);



figure

hold on

plot(time_back_corrected,R_back_start_time_aligned)

plot(time_front_corrected,R_front_start_time_aligned)

xlabel('Time / sec');

ylabel('Resistance / k\Omega');

legend( 'Back','Front')



figure

hold on

plot(time_back_corrected,T_back)

plot(time_front_corrected,T_front)

xlabel('Time / sec');

ylabel('Temperature / C');

legend('Back','Front')
```